Research on Chemical Intermediates (2019) 45:815–832
https://doi.org/10.1007/s11164-018-3645-0

Pd–Co alloy as an efficient recyclable catalyst for the reduction of hazardous 4-nitrophenol

T. A. Revathy, et al. ***[full author details at the end of the article]***

Received: 2 August 2018 / Accepted: 15 October 2018 / Published online: 26 October 2018

Abstract

Palladium–Cobalt (Pd–Co) alloys with different atomic ratios were synthesized successfully by borohydride-assisted chemical reduction method. Pd–Co alloys were characterized to study their physical and chemical properties. Further, the catalytic behavior of the synthesized alloys and effect of cobalt inclusion into alloy for the catalytic behavior was studied using reduction of 4-nitrophenol (4-NP). The reduction of 4-NP into 4-aminophenol by sodium borohydride is one of the eminent model reactions to study catalytic behavior as it enables assessing the catalyst from the kinetic parameters calculated from the real-time spectroscopic monitoring of an aqueous solution. Pd–Co alloys show good catalytic activity towards the reduction of 4-NP and their rate constants were calculated. The catalytic studies reveal that reduction reaction catalyzed by prepared Pd–Co alloys follow the pseudo-first-order kinetics. Among them, $Pd_{26}Co_{74}$ catalyzed the reduction reaction with the minimum time of 7 min having a rate constant of 6.65 ms^{-1}. The turn over frequency (TOF) for the corresponding alloy was calculated and found to be 26 h^{-1}.

Graphical abstract

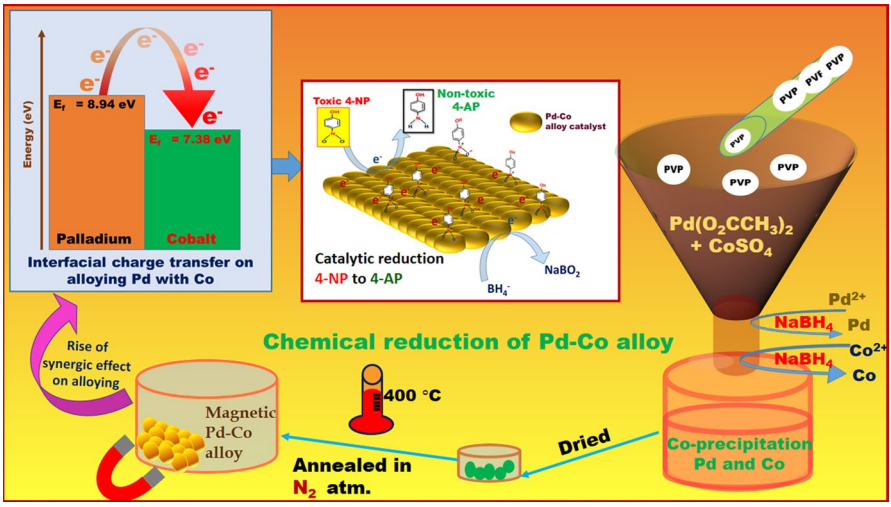

Keywords Pd–Co alloy · Chemical reduction method · Catalysis · Nitrophenol

Introduction

Technological innovation paves the way for new materials with special properties leading to the application of nanomaterial in various fields [1–5]. In recent years, intense research has been adopted by the scientific community to develop highly active catalytic nanomaterial for water treatment for the reduction of various nitro compounds and water-soluble aromatic dyes as these compounds have great impact on both environmental sustainability and human health [6–12]. Nitrophenol is one of the most lethal water toxins. 4-nitrophenol (4-NP) causes serious environmental concern and hence numerous techniques have been adopted for the reduction of these pollutants [13–15]. Among other techniques, conversion of a nitro group into an amine group by hydrogenation is an appropriate way to reduce its toxicity [16–19]. In this way, 4-aminophenol (4-AP), a useful organic compound, can be obtained. Moreover, 4-AP is an important intermediate in manufacturing antipyretic and analgesic drugs like paracetamol, phenacetin and acetanilide [20, 21]. 4-AP is a vital component in the production of industrial dyes, photographic developing techniques and its oxalate salt has been used as a corrosion inhibitor [22–24].

Catalytic reduction of 4-NP by sodium borohydride in the presence of a metal catalyst is found to be a cost-effective and eco-friendly method [25]. Research on noble metal nanoparticles as catalyst is the active topic [26–29]. Among them, palladium has received much attention since it has noticeable characteristic activity as a catalyst for various reactions [30–36]. Even though palladium nanoparticles, as the

best catalyst, exhibit higher surface energy due to large surface-to-volume ratio, the stability of the nanoparticles during the catalytic reaction is compromised because of its higher collision frequency, tendency to aggregate, change in shape and destruction of its surface atoms; this leads to the subsequent loss of its initial activity and selectivity. So, fabricating a proficient and reusable catalyst for the hydrogenation of 4-NP is an interesting task to be accomplished. The highest possibility in tuning and controlling the catalytic activity can be achieved by alloying [37–41]. In alloying, electrons from the metal counterpart with a higher energy level transfer to the metal with low Fermi energy, thereby altering the electronic structure of the alloy. In the case of Pd–Co alloy, electrons from palladium with a Fermi level ($E_f = 8.94$ eV) leap to cobalt ($E_f = 7.38$ eV). The interaction of active sites of a catalyst with hydrogen species is altered due to the interfacial charge transfer from palladium to cobalt. Thus, alloying of palladium with cobalt enhances the catalytic activity. Due to interfacial electron transfer, the d-band center approaches the Fermi level, thereby filling the electron population in the bonding orbitals [42]. Thus, increase in binding energy of the alloy's d-band increases the chemisorption [43]. The enhanced catalytic reduction was induced due to increased transfer of more electrons from borohydride to nitrophenol on the active sites; this is compared to low-lying d-bands with more anti-bonding orbitals, as in individual metals. In particular, when a 4*d* transition metal like palladium having high spin–orbit coupling is alloyed with a 3*d* transition magnetic metal, the catalytic behavior is enhanced [44–47]. The change in geometrical and electronic state on alloying also leads to enhancement of the catalytic behavior of metals [48–51]. In addition to all these advantages, inclusion of magnetic material as one of the alloy components smoothens the separation of the catalyst from reaction medium by external magnetic force and also the catalyst can be reused [52]. These advantages motivate researchers to innovate techniques for enrichment of palladium-based alloys and thus increases its scope in common usage [53, 54].

In this work, synthesis of Pd–Co alloy by the simple and cost-effective sodium borohydride-assisted chemical reduction method is presented with its various characterizations. Catalytic behavior of the Pd–Co alloy towards the reduction of 4-NP was studied. Moreover, the effect on catalytic behavior of Pd–Co alloy with respect to atomic ratio of Co in the alloy was appraised.

Experimental details

Reagents

Palladium acetate (98% pure), cobalt sulfate heptahydrate and polyvinylpyrrolidone (PVP) were procured from Sigma-Aldrich and used in the reaction as received. Ammonia (99% pure) and hydrochloric acid were obtained from Merck. Sodium borohydride and 4-NP were bought from s d fine chemicals and all the

chemicals used in the reported work were of analytical reagent grade. The experiments were carried out using double-distilled water.

Synthesis of Pd–Co alloy

Pd–Co alloys were synthesized by the cost-effective chemical reduction method using sodium borohydride as reducing agent. Palladium precursor solution was prepared by dissolving palladium acetate in distilled water mixed with 1 ml of HCl. The concentration of cobalt sulfate was chosen so that the alloy would have 10, 25, 50, 75 and 90% of cobalt. The mixture of palladium and cobalt precursor solution was stirred for 30 min. Then PVP solution as a stabilizing agent was added in drops to the mixture. The required amount of $NaBH_4$ was added to the above solution and the obtained precipitate was filtered, washed and dried at room temperature. The as-prepared samples were annealed at 400 °C for 2 h under nitrogen atmosphere. The samples were labeled A, B, C, D, E and F with respect to palladium and cobalt composition and the details are given in Table 1.

Characterization

The composition of the alloys were ascertained from atomic absorption spectroscopy (AAS; Perkin Elmer AAS 700). The samples for AAS analysis were prepared by dissolving the alloy in 5 ml of 1:1 mixture of nitric acid and sulfuric acid. Then the solution was diluted to 100 ml using double-distilled water. Powder X-ray diffraction (XRD) analysis was carried out using a GE X-ray diffraction system (XRD 3003 TT) with $CuK\alpha_1$ radiation ($\lambda = 1.5406$ Å). The XRD patterns were obtained from 35° to 80° at 0.04°/s. The chemical environment of the alloy was analyzed using X-ray photoelectron spectroscopy (XPS; DAR400-XM 1000, OMICRON Nanotechnologies, Germany) equipped with dual Al/Mg anodes. The Al anode was used in obtaining the survey and elemental spectra. All spectra were standardized using C 1*s* peak at 284.5 eV to eliminate the charging effect on the sample. The morphologies of the alloys were revealed via high-resolution scanning electron microscopy (HRSEM) equipped with an energy-dispersive X-ray spectrometer (FEI Quanta FEG 200). The transmission electron spectroscopy (TEM) analysis was carried out on a JEOL JEM 2100 instrument operating at 200 keV. The TEM samples were prepared by dispersing the samples in ethanol and then dropping them onto the carbon grid for analysis. Dynamic light scattering (DLS, Malvern Zetasizer, 3000HSa, UK) was used to measure the particle size distribution of the nanoparticles. Selected area electron diffraction (SAED) patterns were constructed at selected regions to study the alloy's structure. Phase transition and thermal stability of the alloys were characterized using differential scanning calorimetry (DSC) and thermo gravimetric analysis (TGA) using a NETZSCH DSC 214 (equipped with TGA). The magnetic behavior of the alloys were studied using vibrating sample magnetometer (VSM, EG&G PARC, Model 4500). The catalytic reduction of 4-NP was observed using a UV–visible spectrometer (Analytik Gena, Specord 210 plus).

Table 1 Stoichiometry of the prepared alloy ascertained from atomic absorption spectroscopy analysis and its label and summary of its structural property

Sample	Sample label	Molar ratio of palladium acetate:cobalt sulfate	Atomic ratios of Pd–Co alloys		Lattice parameter (Å)	Crystallite size ~ (nm)
			Pd %	Co %		
1	A	90:10	89.36	10.64	3.88	4
2	B	75:25	74.44	25.56	3.81	9
3	C	50:50	42.46	57.54	3.86	11
4	D	25:75	26.66	73.34	3.85	6
5	E	10:90	08.60	91.4	3.79	6

Catalytic reduction of 4-NP

To investigate the catalytic activity of the alloy hybrids, the reduction of 4-NP was tested in a quartz cuvette. Aqueous solution of 4-NP (2.8 ml, 0.5 mM) was added to the cuvette. The obtained 4-NP solution had a noticeable light-yellow shade. After adding 400 µl of freshly prepared 30 mM $NaBH_4$, the absorption peak was red-shifted to 400 nm from 317 nm (absorption of 4-NP) and the change in color from light yellow to bright yellow was observed rapidly, confirming the 4-nitrophenolate anion formation. Prepared Pd–Co alloy (0.2 mg) was added to the quartz cuvette. The color of the solution changed gradually from bright yellow to colorless and, consequently, a gradual decrease in the peak intensity centered at 400 nm was observed; this decrease in the intensity clearly indicated the subsequent reduction of 4-NP. The catalytic activities of Pd–Co alloys prepared with different atomic ratios were studied. The catalytic activity of Pd–Co alloys of all compositions were compared. The catalytic process was monitored at ambient condition using an UV–Vis spectrophotometer in the range 250–550 nm at regular time intervals.

Result and discussions

Compositional analysis

The atomic composition of alloys were obtained from AAS analysis and are listed in Table 1. It was observed that alloy compositions were formed with respect to the initial concentration of the bath.

Structural analysis

Figure 1 presents the XRD pattern of Pd–Co alloys with different atomic ratios. The pattern show that the position and relative intensities of all the diffraction peaks match well with the standard pattern of Pd–Co alloy. The three diffraction peaks positioned at 41.59°, 48.52° and 71.1° were respectively attributed to the (111), (200) and (220) diffraction planes which were persistent with the standard XRD data for the face-centered

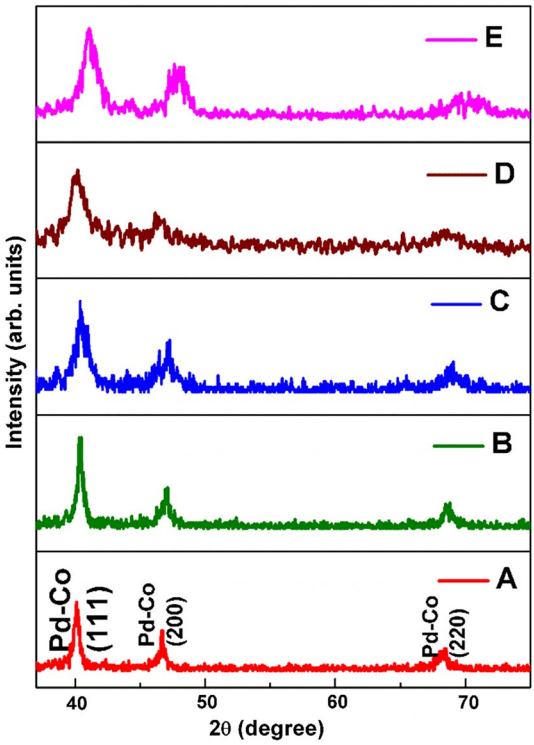

Fig. 1 XRD pattern of Pd–Co alloys

cubic (FCC) Pd–Co alloy (JCPDS card file no. 65-6075). It was observed from the graph that as the composition of cobalt was increased in the prepared alloy, the diffraction peaks were slightly shifted to higher 2θ values. This shift in angle is due to decrease in the size of the lattice parameter on incorporation of cobalt with palladium.

The lattice parameters of the alloys were estimated from the XRD patterns, and the average crystallite size of the alloys were evaluated by Scherrer's formula. The calculated lattice parameters are presented in Table 1. The average crystallite size of Pd–Co alloys having different atomic ratios vary from 4 to 11 nm. On increasing the cobalt content in the alloy, values of lattice parameters decrease. The results clearly showed that there was a change in the geometry of the crystal structure in the prepared alloys. This geometric effect influences the interaction between adsorbed species and the surface atoms by means of its atomic arrangement in the active surface site [55]. As such, change in the geometry arose due to the lattice compression enhancing the catalytic property of the prepared Pd–Co alloy catalysts [43].

The elemental state as well as the chemical contents of the alloy were examined using XPS. The presence of palladium and cobalt, which corresponds to Pd–Co alloy (sample D) devoid of impurities, as confirmed from the survey spectrum is shown in Fig. 2a. High-resolution spectra of Pd and Co present in the alloy are shown in Fig. 2b, c, respectively. The doublet peak of Pd was deconvoluted into four peaks allied to $Pd^0(3d_{5/2})$, $Pd^{2+}(3d_{5/2})$, Pd^0 $(3d_{3/2})$ and Pd^{2+} $(3d_{3/2})$ with binding energies around 335.7, 338.4, 341.3 and 343.8 eV, respectively. The binding energy peaks at

335.7 and 341.3 eV correspond to the metallic palladium peaks with slight increase in the binding energy when compared to that of binding energy peak of pure Pd aroused at 335.5 eV [43, 44]. The shift in binding energy was due to the electronic interaction between palladium and cobalt as an effect of alloying palladium with cobalt. This increase in binding energy of the d-band of the alloy increases the tendency of interaction of adsorbents when compared to low-lying d-bands with more anti-bonding orbitals. The change in electronic structure during the formation of an alloy enhances the catalytic behavior of the alloy [56, 57]. Also, two peaks at binding energies of 338.4 and 343.8 eV may be aroused due to the surface oxidation (Pd^{2+} state) of the sample.

Similarly for cobalt spectrum, the peak was again deconvoluted into four peaks. The doublet peak of Co was deconvoluted into four peaks corresponding to Co^0 ($3d_{5/2}$), Co^{2+} ($3d_{5/2}$), Co^0 ($3d_{3/2}$) and Co^{2+} ($3d_{3/2}$) with binding energies at 782.7, 789, 798.4 and 805 eV, respectively. Binding energies of both Pd^0 (335.5 eV) and Co^0 (778.2 eV) peaks are shifted from pure palladium and cobalt, suggesting the alloy formation between these two elements [58–61]. The atomic fraction of elements (C_x) in the alloy can be calculated using the general expression:

$$C_x = \frac{\frac{A_x}{S_x}}{1 \quad \frac{A_x}{S_x}}$$

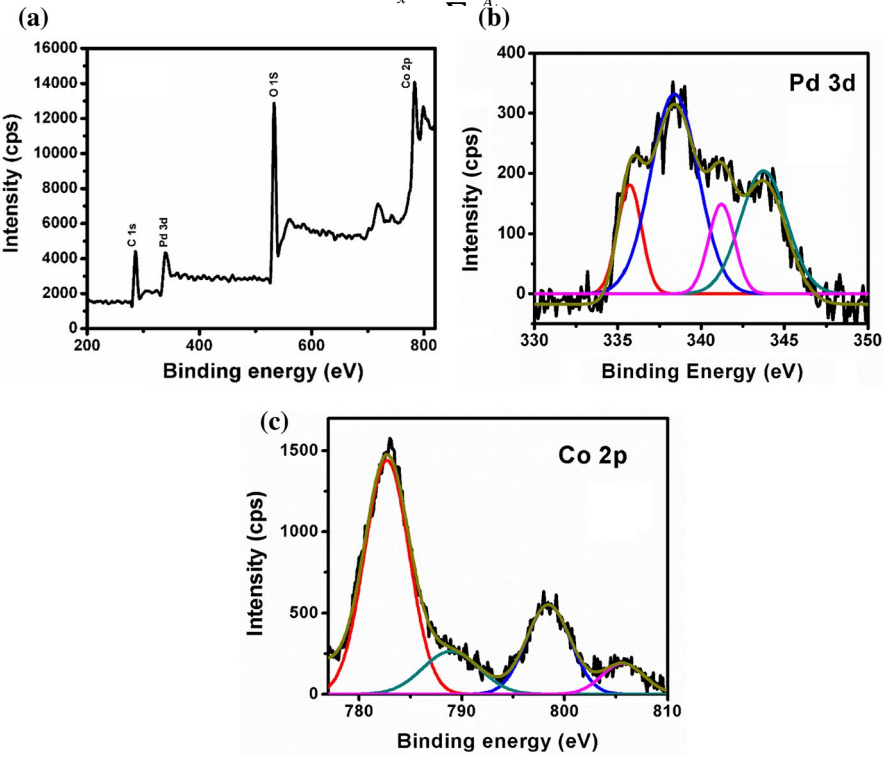

Fig. 2 Survey scan XPS spectrum of Pd–Co alloy (sample D) and its high-resolution spectra of Pd 3*d* and Co 2*p*

where A is the peak area and S is the atomic sensitivity factor.

The atomic percentages of Pd and Co in alloy are found to be 25.18 and 74.81%, respectively, which correlates with the atomic ratio ascertained from AAS analysis.

Morphological studies

The densely packed leaf like morphology of the particles were observed in the HRSEM image and shown in Fig. 3. The micrograph clearly shows that the particles grow to make densely packed leaf like shapes. A slight change in the morphology of the alloys was noted with respect to their atomic ratio. The morphology changes from leaf to spheres as cobalt content increases in alloy, wherein the nanospheres tend to arrange linearly like a rod in morphology.

HRTEM images of the alloy (sample D) are shown in Fig. 4a–c with lower and higher magnification respectively. Micrographs of the alloy depicts that the particles were homogenously distributed. Figure 4c depicts the lattice fringe spacing of ~0.213 nm, ~0.189 nm, ~0.138 nm observed from the particles were indexed to the (111), (200) and (220) planes of *FCC* structured Pd–Co alloy and concurred with the standard JCPDS value of Pd–Co alloy.

The obtained d-spacing values additionally ensured the formation of Pd–Co alloy in coherence with XRD analysis. Figure 4d shows the SAED pattern of sample D. The interplanar d-spacing values for diffracted rings were calculated and was observed that the spacing values matches with the $d_{(111)}$, $d_{(200)}$, $d_{(220)}$ and $d_{(311)}$ of Pd–Co FCC structure with reference to the JCPDS number 65-6075. The obtained SAED data was found to be consistent with the XRD results.

In Fig. 5a, the size distribution histogram of the Pd–Co alloy were obtained from a randomly selected area of the HRTEM image is shown. From the histogram, it is established that the average particles size were ~10.5 nm. The particle size distribution of the alloy was done using DLS as shown in Fig. 5b. The average particles size of Pd–Co alloy (sample D) were observed to be ~11 nm and was in good agreement with particles size of alloy estimated from HRTEM analysis.

Magnetic studies

Magnetization as a function of the applied field $M(H)$ is shown in Fig. 6. It shows that Pd–Co alloys exhibit well-defined hysteresis loops, while the magnetic response of the Pd–Co alloy with low cobalt content to the applied field was weak, as in a weak ferromagnetic material.

Table 2 depicts the comparison of the saturation magnetization (M_s), retentivity (M_r), coercivity (H_c), squareness ratio, switching field distribution (SFD) value and hysteresis loss of all the samples along with the respective Co content in the alloy. The magnetic characterization shows that Pd–Co alloys are ferromagnetic in nature and the value of the magnetization saturation can be positively associated with the cobalt content in the alloys. From the squareness ratio, it was found that all the

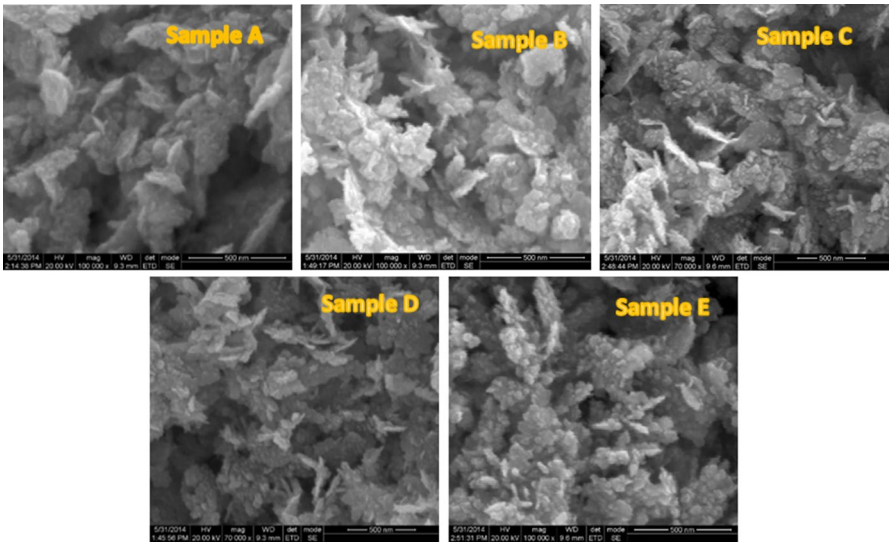

Fig. 3 HRSEM images of Pd–Co alloys prepared with different atomic ratios

alloys have pseudo-single-order domains. Pd–Co alloys are hence suitable for use as ferromagnetic electrodes and other applications.

Thermal analysis

The phase transition of the Pd–Co alloy (sample D) was studied using DSC analysis and is shown in Fig. 7 and the inset of Fig. 7 shows the thermal stability of the alloy examined by TGA analysis. The DSC thermogram of Pd–Co alloy indicates the presence of both exothermic and endothermic peaks that resulted from the changes in structure of the alloy with temperature. The endothermic peak observed at 149 °C was due to dehydrogenation of adsorbed water molecules on the surface of the alloy [46]. The amount of enthalpy absorbed during dehydrogenation was calculated from the thermograph and it was found to be 2.7 kJ/g. Dehydrogenation was also evident from the TGA analysis since there was an apparent loss in mass around 150 °C. The second peak was an exothermic peak with onset around 360 °C which corresponds to crystallization of Pd–Co alloy. The amount of enthalpy evolved during this transition is 38 kJ/g. Structural phase formation was evident from the XRD analysis; in the as-prepared condition, the sample showed an amorphous nature and on annealing at 400 °C, Pd–Co alloy with an FCC crystal structure was formed.

Catalytic behavior

Reduction of 4-NP into 4-AP by sodium borohydride was carried out with the aim of evaluating the catalytic behavior of Pd–Co alloy. The reduction process was monitored using UV–Vis absorbance spectroscopy and is shown in Fig. 8. On the

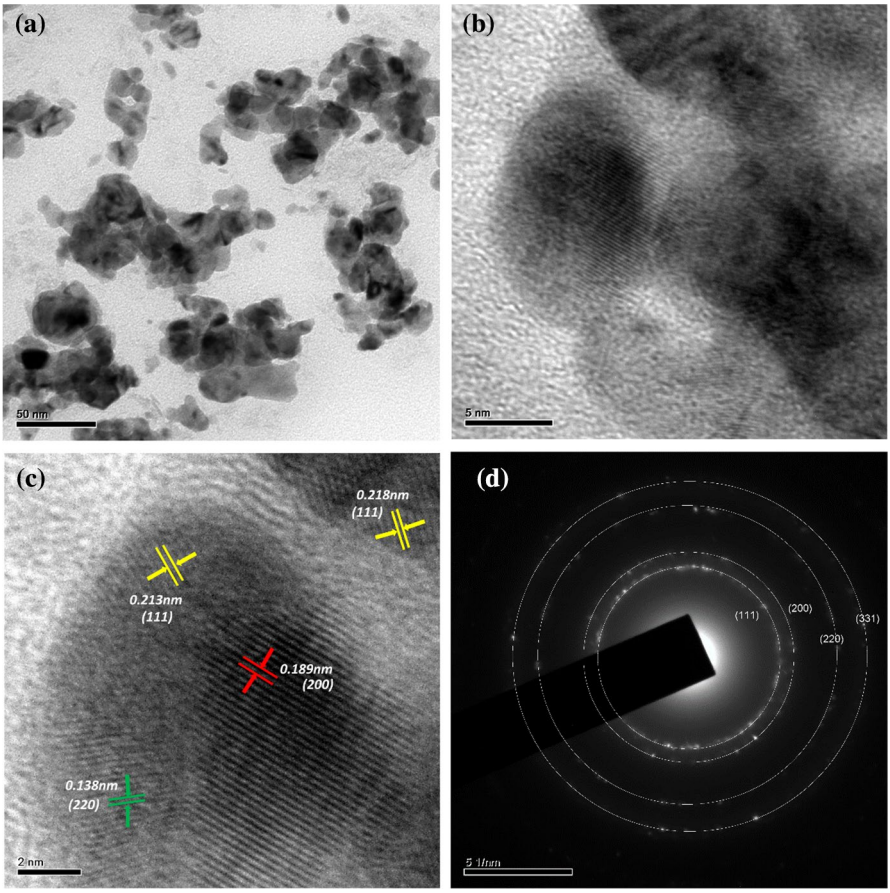

Fig. 4 HRTEM images of Pd–Co alloy with lower magnification (**a**) and higher magnification (**b**, **c**) and selected area electron diffraction pattern (**d**)

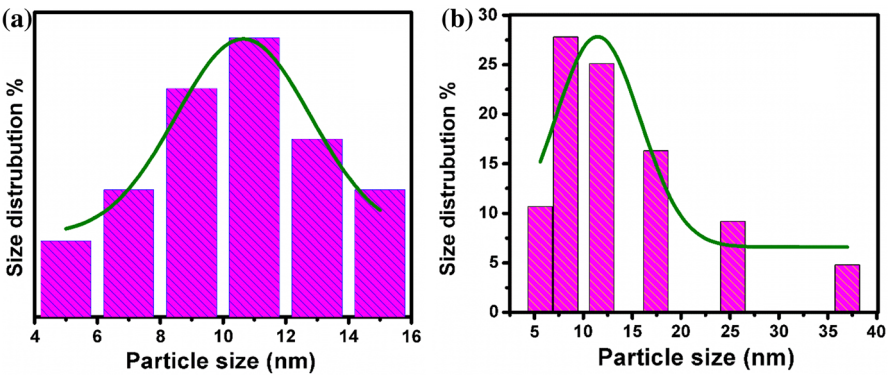

Fig. 5 Particle size histograms of Pd–Co alloy from **a** HRTEM analysis and **b** DLS

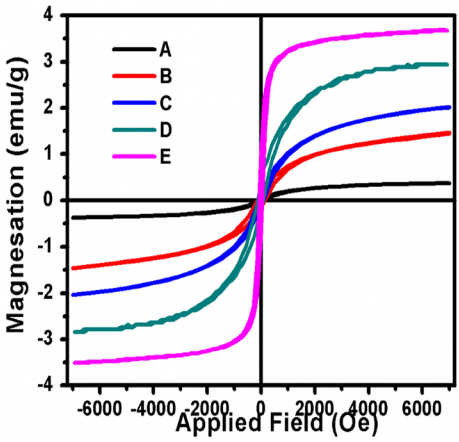

Fig. 6 Magnetic response of Pd–Co alloys

Table 2 Magnetic behavior of Pd–Co alloys

Sample	Co content (at.%)	M_s (emu/g)	M_r (emu/g)	H_c (Oe)	M_r/M_s	SFD	Hysteresis loss (Am^2/kg. cycle)
A	10	0.37	0.02	97	0.05	11.3	90
B	25	1.44	0.14	144	0.09	19.5	362
C	50	2.02	0.12	92	0.08	12.3	344
D	75	2.37	0.76	150	0.32	11.1	948
E	90	2.6	0.94	135	0.26	10.7	1024

addition of sodium borohydride, the characteristic peak observed at 317 nm corresponding to 4-NP shifted to 400 nm due to the formation of nitrophenolate ions. Further, the change in color of the solution from light yellow to dark yellow also indicates that nitrophenolate ions are formed. The reduction of phenolate ion to aminophenol is a very slow process. It can even take several days to reduce completely. In order to intensify the electron transfer from reducing agent to the 4-NP, the catalyst was added to the reaction medium. On the addition of Pd–Co alloy as a catalyst, the absorption intensity of phenolate ion at 400 nm starts to decrease in succession with respect to time.

Concurrently, a new peak was observed at 300 nm which corresponds to 4-AP. The conversion of 4-NP into 4-AP can be simply overseen by an UV–Vis spectrophotometer scan as shown in Fig. 8. Kinematics of the reduction reaction using the Pd–Co alloy with different atomic ratios as the catalyst were examined from $\ln(C/C_0)$ vs. time graph and these graphs are given as the inset in the corresponding absorption plot. The reduction reaction rate constant (k) was deduced from slope of the kinetic plot. The catalytic behavior of all the alloy samples and pure Co towards the reduction of 4-NP are tabulated for comparison and presented in Table 3.

On correlation of the results, sample D ($Pd_{26}Co_{74}$) showed splendid catalytic activity in comparison with other alloys. As the cobalt content increased, more

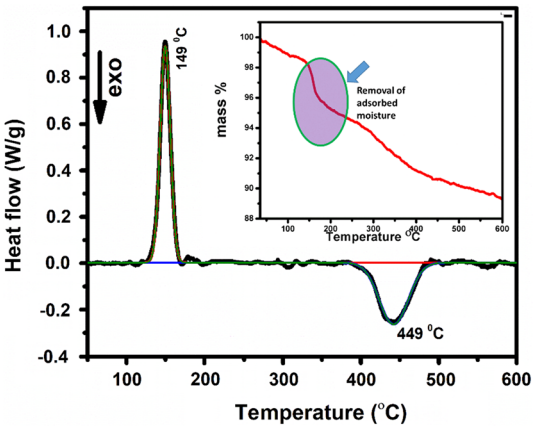

Fig. 7 DSC thermogram of Pd–Co alloy (sample D)

nanospheres tend to remain on the surface of the alloy, as depicted by morphological analysis. The spherical particles lead to more active sites on the surface, availing places for hydrogen adsorption. Even with the low concentration of Pd, all Pd–Co alloys exhibit enhanced catalytic activity when compared to pure Pd. The above results show that the reduction of 4-NP catalyzed by Pd–Co alloy was done in a minimum time of 7 min at a rate constant of 6.65 ms^{-1}. On analyzing the kinetic curve, it is clear that reduction reactions comply with the pseudo-first-order reaction mechanism. The turnover frequency of the catalyst (sample D) was calculated and found to be ~ 26 h^{-1}.

For practical consideration of alloy for usage as a catalyst, $Pd_{26}Co_{74}$ was subjected to stability and reusability tests. After the reduction of 4-NP, Pd–Co alloy was separated using an external magnetic field from the reaction medium and the catalyst was reused for for four more new reduction processes. The reliability and stability of the prepared alloy is shown in Fig. 9. The stability of the alloy remained unaltered for three cycles of reduction, and after the third cycle, the kinetic rate constant k value started to decrease.

The possible reduction mechanism of 4-NP to 4-AP catalyzed by Pd–Co alloy is schematically represented in Fig. 10. Alloying palladium with cobalt modified the structural properties and electronic structure and thus increased the number of unsaturated active sites for hydrogen adsorption onto the catalyst. The adsorption of reactant ions onto the catalyst surface helps the reduction reaction to overcome its kinetic barrier during the reaction and hence increases the rate of reduction. The catalytic process may involve few steps as follows: adsorption of 4-NP ion on to the surface of the Pd–Co alloy; at the same time, the BH_4^- from sodium borohydride is also adsorbed onto the Pd–Co alloy; At this point, Pd–Co alloy initiates the electron transfer between BH_4^- anion and the 4-NP ion, i.e., the catalyst receives the electron pair dissociated from the BH_4^- anion and supplies it to the nitrophenolate ion; this resulted in hydrogenation of the nitro group present in the 4-NP forming ecofriendly 4-AP molecules as the reaction product.

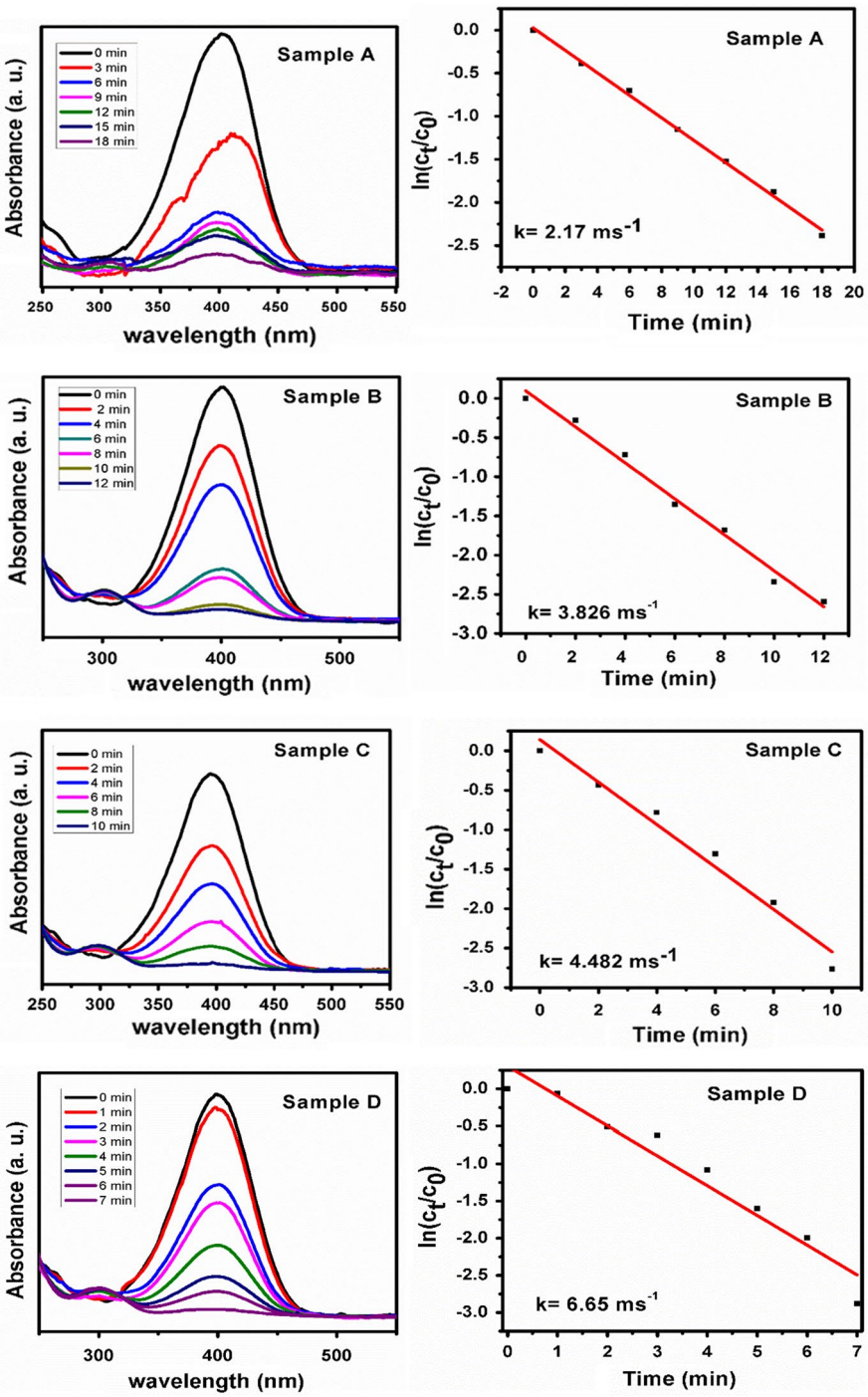

Fig. 8 UV–Vis spectra for the reduction 4-nitrophenol using Pd–Co alloys and cobalt catalyst respectively and its corresponding reaction kinetics plot of conversion

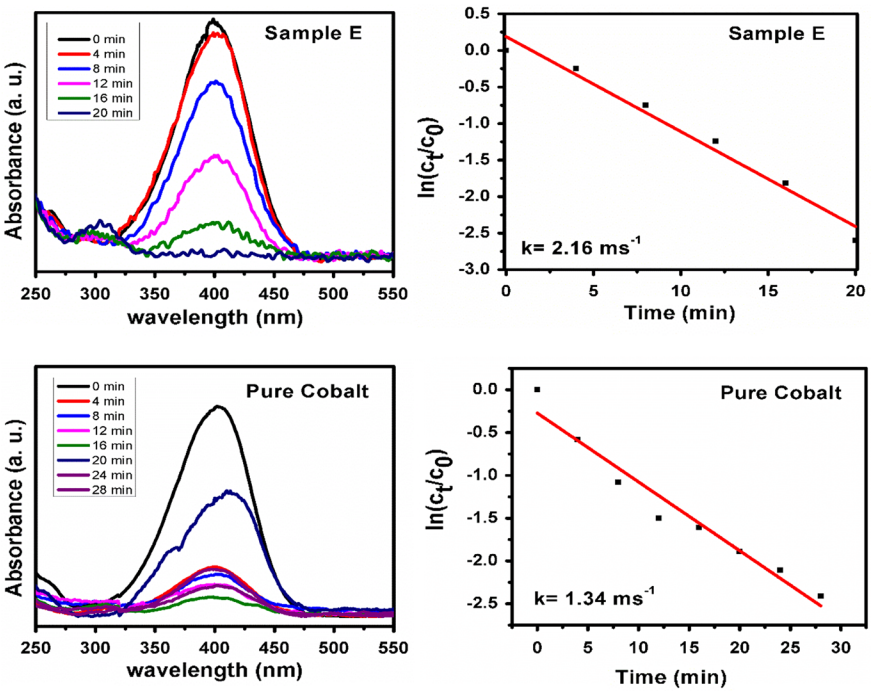

Fig. 8 (continued)

Table 3 Catalytic activity of Pd–Co alloy

Sample	Sample	Time (min)	Rate constant (ms^{-1})
1	A	18	2.17
2	B	12	3.82
3	C	10	4.48
4	D	7	6.65
5	E	20	2.16
6	Cobalt	28	1.34

Recent literature reports on 4-NP reduction catalyzed by various nanoparticles are listed in Table 4. The present work was compared with the previous reports. 4-NP reduction using Pd–Co alloy as a catalyst showed superior catalytic behavior.

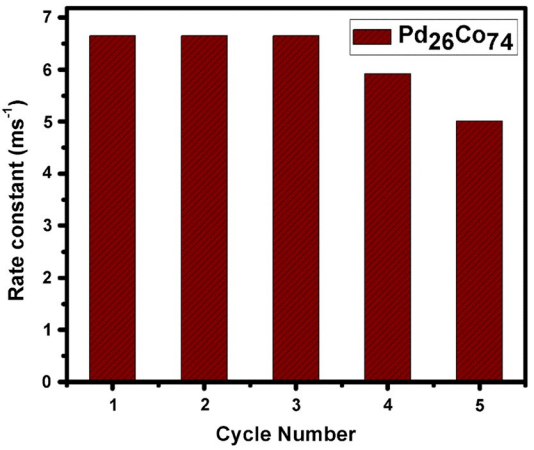

Fig. 9 Reliability and stability of Pd–Co alloy

Conclusion

Pd–Co alloys were successfully synthesized using the chemical reduction method with various atomic ratios, and the effect of cobalt inclusion into the alloy for the catalytic behavior towards the 4-NP was elaborated. The formation of an FCC structured alloy with geometrical effect was confirmed by XRD analysis which was also noticeable in SAED patterns. Addition of cobalt induces the magnetic effect in the catalyst, making it more suitable for reuse. The effect of cobalt content on catalytic activity of Pd–Co alloys towards the reduction of 4-NP were studied. The predictable kinetic rate constant of Pd–Co alloys indicates that the catalytic activity of the alloys was enhanced when compared with pure components. Enhancement of the

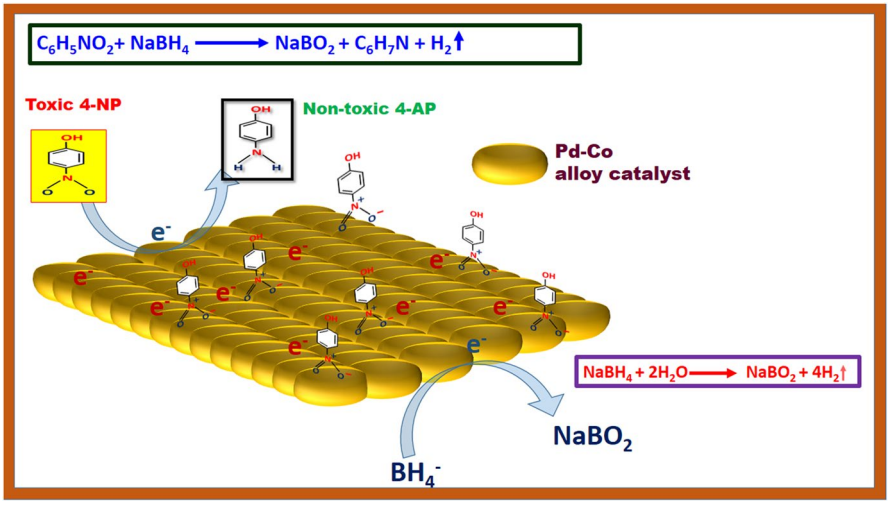

Fig. 10 Schematic representation of catalytic reduction of 4-nitrophenol to 4-aminophenol

Table 4 Recent report on catalytic behavior of 4-nitrophenol

Material	Catalytic conditions (room temperature, cuvette)				
	Mass (mg)	4-NP (mM)	$NaBH_4$ (mM)	k (ms^{-1})	References
Co	3	0.001	0.02	3.51	[62]
Au/SBA-15	2.1	0.2	15	3.24	[63]
Ni@Pd/KCC	10	500	0.12	0.2	[64]
Pd/Fe3O4@ SiO2@KCC-1	5	10	50	0.19	[65]
Pd/G	4	0.3	100	2.4	[66]
Pd–Co alloy	0.2	0.5	30	6.65	This work

catalytic activity of alloys was due to the synergistic effect induced because of the interfacial charge transfer from palladium to cobalt and structural modification in the alloy.

Acknowledgements One of the authors, T. A. Revathy, acknowledges UGC-UPE-Phase II for the financial assistance as a fellowship. Authors thank Dr. J. Senthil Selvan, Department of Nuclear physics, University of Madras, for access to UV–Vis absorption spectroscopy and K. C. Dharani Balaji, IIT Madras, is also acknowledged for HRSEM measurements.

Compliance with ethical standards

Conflict of interest There are no conflicts of interest to declare.

References

1. S. Wang, R. Su, S. Nie, M. Sun, J. Zhang, D. Wu, N. Moustaid-Moussa, J. Nutr. Biochem. **25**, 363 (2014)
2. K. Duygu, Y. Shimeng, H.S.P. Wong, Nanotechnology **24**, 382001 (2013)
3. X. Qu, P.J.J. Alvarez, Q. Li, Water Res. **47**, 3931 (2013)
4. Q.A. Pankhurst, J. Connolly, S.K. Jones, J. Dobson, J. Phys. D Appl. Phys. **36**, R167 (2003)
5. N.N. Nassar, A. Hassan, P. Pereira-Almao, Energy Fuels **25**, 1566 (2011)
6. X.-L. Chen, B.-R. Ai, Y. Dong, X.-M. Zhang, J.-Y. Wang, Tetrahedron Lett. **58**, 3646 (2017)
7. T.B. Devi, M. Ahmaruzzaman, Mater. Today Proc. **5**, 2098 (2018)
8. P. Zhou, Z. Zhang, L. Jiang, C. Yu, K. Lv, J. Sun, S. Wang, Appl. Catal. B **210**, 522 (2017)
9. G. Singh, S. Rani, A. Arora, Sanchita, H. Duggal, D. Mehta, Mol. Catal. **431**, 15 (2017)
10. D. Nandi, S. Siwal, M. Choudhary, K. Mallick, Appl. Catal. A **523**, 31 (2016)
11. L. Cisneros, P. Serna, A. Corma, Chin. J. Catal. **37**, 1756 (2016)
12. K. Ikehata, M. Gamal El-Din, S.A. Snyder, Ozone Sci. Eng. **30**, 21 (2008)
13. Prateek, C. Thakur, C. Srivastava Vimal, D. Mall Indra, Int. J. Chem. Reactor Eng. **11**, 595 (2013)
14. W. Shen, Y. Qu, X. Pei, S. Li, S. You, J. Wang, Z. Zhang, J. Zhou, J. Hazard. Mater. **321**, 299 (2017)
15. S. Jaerger, A. dos Santos, A. N. Fernandes, C. A. P. Almeida, Water Air Soil Pollut. **226**, 236 (2015)
16. L.L. Bo, Y.B. Zhang, X. Quan, B. Zhao, J. Hazard. Mater. **153**, 1201 (2008)
17. M.A. Oturan, J. Peiroten, P. Chartrin, A.J. Acher, Environ. Sci. Technol. **34**, 3474 (2000)
18. P. Cañizares, C. Sáez, J. Lobato, M.A. Rodrigo, Ind. Eng. Chem. Res. **43**, 1944 (2004)
19. M.S. Dieckmann, K.A. Gray, Water Res. **30**, 1169 (1996)
20. M.S. Bloomfield, Talanta **58**, 1301 (2002)
21. A. Roy, B. Debnath, R. Sahoo, T. Aditya, T. Pal, J. Colloid Interface Sci. **493**, 288 (2017)

22. J.O. Otutu, D. Okoro, E.K. Ossai, J. Appl. Sci. **8**, 334 (2008)
23. H.M. Pinheiro, E. Touraud, O. Thomas, Dyes Pigm. **61**, 121 (2004)
24. N.A. Penner, P.N. Nesterenko, Analyst **125**, 1249 (2000)
25. A. Fedorczyk, J. Ratajczak, O. Kuzmych, M. Skompska, J. Solid State Electrochem. **19**, 2849 (2015)
26. K. Suwannarat, K. Thongthai, S. Ananta, L. Srisombat, Colloids Surf. A **540**, 73 (2018)
27. L. Srisombat, J. Nonkumwong, K. Suwannarat, B. Kuntalue, S. Ananta, Colloids Surf. A **512**, 17 (2017)
28. P. Xu, C. Cen, N. Chen, H. Lin, Q. Wang, N. Xu, J. Tang, Z. Teng, J. Colloid Interface Sci. **526**, 194 (2018)
29. H. Guan, C. Chao, Y. Lu, H. Shang, Y. Zhao, S. Yuan, B. Zhang, J. Chem. Sci. **128**, 1355 (2016)
30. B.P. Chaplin, M. Reinhard, W.F. Schneider, C. Schüth, J.R. Shapley, T.J. Strathmann, C.J. Werth, Environ. Sci. Technol. **46**, 3655 (2012)
31. Á. Molnár, Chem. Rev. **111**, 2251 (2011)
32. C.J. Calderón Gómez, R. Moliner, J.M. Lázaro, Catalysts **6**, 130 (2016)
33. S. Dhanavel, N. Manivannan, N. Mathivanan, V.K. Gupta, V. Narayanan, A. Stephen, J. Mol. Liq. **257**, 32 (2018)
34. S. Dhanavel, E.A.K. Nivethaa, G. Esther, V. Narayanan, A. Stephen, AIP Proc. **1731**, 050092 (2016)
35. S. Dhanavel, T.A. Revathy, A. Padmanaban, V. Narayanan, A. Stephen, J. Mater. Sci Mater. Electron. **29**, 14093 (2018)
36. X. Yang, J.-K. Sun, M. Kitta, H. Pang, Q. Xu, Nat. Catal. **1**, 214 (2018)
37. A.A.S. Nair, R. Sundara, J. Phys. Chem. C **120**, 9612 (2016)
38. B. Coq, F. Figueras, J. Mol. Catal. A Chem. **173**, 117 (2001)
39. K. Dhanapal, T.A. Revathy, S. Dhanavel, V. Narayanan, A. Stephen, Surfaces Interfaces **7**, 58 (2017)
40. J. Yang, W.D. Wang, Z. Dong, J. Colloid Interface Sci. **524**, 84 (2018)
41. A.K. Singh, Q. Xu, ChemCatChem **5**, 652 (2013)
42. Y. Peng, B. Lu, N. Wang, L. Li, S. Chen, PCCP **19**, 9336 (2017)
43. E. Toyoda, R. Jinnouchi, T. Hatanaka, Y. Morimoto, K. Mitsuhara, A. Visikovskiy, Y. Kido, J. Phys. Chem. C **115**, 21236 (2011)
44. J.D. Aiken, R.G. Finke, J. Mol. Catal. A Chem. **145**, 1 (1999)
45. J. Krajczewski, K. Kołątaj, A. Kudelski, Appl. Surf. Sci. **388**, 624 (2016)
46. H. Lu, H. Yin, Y. Liu, T. Jiang, L. Yu, Catal. Commun. **10**, 313 (2008)
47. H. Guan, C. Chao, W. Kong, Z. Hu, Y. Zhao, S. Yuan, B. Zhang, J. Nanopart. Res. **19**, 187 (2017)
48. F. Yang, D.L. Zhao, Mater. Sci. Forum **475–479**, 3107 (2005)
49. F.J.C.M. Toolenaar, F. Stoop, V. Ponec, J. Catal. **82**, 1 (1983)
50. A.E. Baber, H.L. Tierney, E.C.H. Sykes, ACS Nano **4**, 1637 (2010)
51. T.A. Revathy, K. Dhanapal, S. Dhanavel, V. Narayanan, A. Stephen, J. Alloys Compd. **735**, 1703 (2018)
52. Y. Zhong, Y. Gu, L. Yu, G. Cheng, X. Yang, M. Sun, B. He, Colloids Surf. A **547**, 28 (2018)
53. F. Li, Y. Liu, T. Ma, D. Xu, X. Li, G. Gong, New J. Chem. **41**, 4014 (2017)
54. T. Vats, S. Dutt, R. Kumar, P.F. Siril, Sci Rep. **6**, 33053 (2016)
55. M. Ma, H.A. Hansen, M. Valenti, Z. Wang, A. Cao, M. Dong, W.A. Smith, Nano Energy **42**, 51 (2017)
56. D. Kim, J. Resasco, Y. Yu, A.M. Asiri, P.D. Yang, Nat. Commun. **5**, 4948 (2014)
57. N. Palina, O. Sakata, L.S.R. Kumara, C. Song, K. Sato, K. Nagaoka, T. Komatsu, H. Kobayashi, K. Kusada, H. Kitagawa, Sci Rep. **7**, 41264 (2017)
58. M. Krawczyk, J.W. Sobczak, Appl. Surf. Sci. **235**, 49 (2004)
59. P. Chandran, A. Ghosh, S. Ramaprabhu, Sci. Rep. **8**, 3591 (2018)
60. K.X. Zhu, C.Z. Jin, Z. Klencsar, A.S. Ganeshraja, J.H. Wang, Catalysts **7**, 138 (2017)
61. M.A. Matin, J.-H. Jang, Y.-U. Kwon, J. Power Sour. **262**, 356 (2014)
62. A. Mondal, A. Mondal, B. Adhikary, D.K. Mukherjee, Bull. Mater. Sci. **40**, 321 (2017)
63. S.M. El-Sheikh, A.A. Ismail, J.F. Al-Sharab, New J. Chem. **37**, 2399 (2013)
64. Z. Dong, X. Le, C. Dong, W. Zhang, X. Li, J. Ma, Appl. Catal. B **162**, 372 (2015)
65. X. Le, Z. Dong, Y. Liu, Z. Jin, T.-D. Huy, M. Le, J. Ma, J. Mater. Chem. A **2**, 19696 (2014)
66. J. Sun, Y. Fu, G. He, X. Sun, X. Wang, Catal. Sci. Technol. **4**, 1742 (2014)

Affiliations

T. A. Revathy[1] · T. Sivaranjani[1] · A. A. Boopathi[2,3] · Srinivasan Sampath[4] · V. Narayanan[5] · A. Stephen[1]

✉ A. Stephen
stephen_arum@hotmail.com

[1] Department of Nuclear Physics, University of Madras, Guindy Campus, Chennai, Tamil Nadu 600025, India

[2] Polymer Science and Technology Division, Council of Scientific and Industrial Research–Central Leather Research Institute, Chennai, India

[3] Academy of Scientific and Innovative Research (AcSIR), New Delhi, India

[4] Department of Materials Science, School of Technology, Central University of Tamil Nadu, Thiruvarur, India

[5] Department of Inorganic Chemistry, University of Madras, Guindy Campus, Chennai, Tamil Nadu 600025, India